Carbohydrate Polymers 99 (2014) 817–824

Contents lists available at ScienceDirect

Carbohydrate Polymers

journal homepage: www.elsevier.com/locate/carbpol

Novel chitosan-ZnO based nanocomposites as luminescent tags for cellulosic materials

Saeed El-Sayed Saeed[a,*], Mohamed M. El-Molla[b], Mohammad L. Hassan[c], Esam Bakir[d], Mohamed M.S. Abdel-Mottaleb[e], Mohamed S.A. Abdel-Mottaleb[d]

[a] Department of Forgery and Counterfeiting Research, Forensic Medicine Authority, Ministry of Justice, El-Sayeda Zeinab, 11461 Cairo, Egypt
[b] Dyeing and Printing Department, Textile Research Division, National Research Center, El-behoos Street, Dokki, 12622 Cairo, Egypt
[c] Cellulose and Paper Department & Advanced Materials and Nanotechnology Group, Centre of Excellence for Advanced Sciences, National Research Center, El-behoos Street, Dokki, 12622 Cairo, Egypt
[d] Nanophotochemistry and Solarchemistry Labs, Department of Chemistry, Faculty of Science, Ain Shams University, Abbassia, 11566 Cairo, Egypt
[e] Center for Nanotechnology, School of Engineering and Applied Sciences, Nile University, Smart Village, K28, Cairo/Alex Desert Road, Cairo, Egypt

ARTICLE INFO

Article history:
Received 7 June 2013
Received in revised form 26 August 2013
Accepted 30 August 2013
Available online 6 September 2013

Keywords:
Luminescent tags
Security features
Eu^{3+} doped chitosan-ZnO
Nanocomposites
Quantumdots
Cellulose

ABSTRACT

Novel chitosan-ZnO composites have been synthesized as luminescent taggants for cellulosic materials. The synthesized chitosan-ZnO nanospheres (CS-ZnO NS), chitosan-ZnO-oleic acid quantum dots (CS-ZnO-oleic QD) and chitosan-ZnO-oleic acid:Eu^{3+} doped nanorods (CS-ZnO-oleic:Eu^{3+} NR) were characterized by X-ray diffraction, photoluminescence spectroscopy, FTIR spectroscopy and transmission electron microscopy. The prepared luminescent CS-ZnO composites were used in printing paste and applied to different types of papers and textiles by using screen printing technique. The colorimetric values of the printed CS-ZnO-oleic acid and CS-ZnO-oleic:Eu^{3+} showed that printing caused slightly change in color values. Scanning electron microscopy images and color values of the printed surface showed that CS-ZnO-oleic QD and highly luminescence CS-ZnO-olic:Eu^{3+} NR are suitable for use as a printed security feature.

1. Introduction

Luminescent tagging of cellulose can be used in many products, e.g., passports, tamper evident labels, postage stamps, identity cards, banknotes, military clothes (Hardwick, Jackson, Wilson, & Mau, 2001; Morrison, 2009; Prime & Solomon, 2010).

The luminous security ink is used for the purpose of prevention forgery or reproduction of recording secret information. The security ink is invisible under visible light, but when being irritated with ultraviolet rays, it emits light and the recorded information can be read. There are few published studies on security ink composites which are based on different organic dye, e.g., poly(methyl methacrylate) composite dyes (Wang, Xu, & Xu, 2011; Wang, Yang, & Yang, 2011). Different Europium complexes based on heterocyclic, fluorohydrocarbon groups (Ikeda, Kitayama, Kiyoyanagi, & Shirasaki, 2006), thenoyltrifluoroacetone and fluorine-comprising alkyl studied as luminous security ink (Imanishi & Yamasaki, 2003). Also Lanthanide complexes used as security ink (Hall-Goulle, 2006), but there isn't any study on europium chitosan-ZnO composite.

Lack of published information on research carried out in this area, has motivated us to explore the utilization of nanomaterials, with unique features (Chan et al., 2002; Mosquera et al., 2013; Smith & Nie, 2010; Wang, Xu, et al., 2011; Wang, Yang, et al., 2011), as taggants for cellulosic materials.

In this paper, we report the synthesis, characterization, and evaluation of the novel luminescent tagging nanocomposites: CS-ZnO, CS-ZnO-oleic acid and CS-ZnO-oleic acid doped with Eu^{3+}. Varying ratios of ZnO, oleic acid and Eu^{3+} were added to chitosan to form these materials. The primary amine and hydroxyl groups are important in the incorporation of ZnO onto chitosan (Muzzarelli, 2011; Riva et al., 2011).

2. Materials and methods

2.1. Materials

2.1.1. Cellulosic materials

White papers (80 g/m^2) were supplied by Xerox (Giza, Egypt), and Quena Paper Industry Company (Kous, Quena, Egypt).

Rakta absorbing paper (stencil printing paper) (70 g/m^2) was supplied by Rakta Paper Manufacturing Company (Abukeer, Alexandria, Egypt).

* Corresponding author. Tel.: +20 1006906469.
E-mail address: saiedelsayed2@yahoo.com (S.E. Saeed).

0144-8617/$ – see front matter © 2013 Elsevier Ltd. All rights reserved.
http://dx.doi.org/10.1016/j.carbpol.2013.08.096

100% scoured and bleached cotton fabric (160 g/m^2) was supplied by Mahalla Misr Spinning and Weaving Company (Mahalla, Egypt).

100% scoured and bleached linen (300 g/m^2) was supplied by the Egyptian Co. for Textile Industry/Dintex, Cairo, Egypt.

2.1.2. Chemicals

High molecular weight chitosan, polyvinyl alcohol, ZnO and Europium (III) nitrate pentahydrate supplied by Sigma–Aldrich (Steinheim, Germany). Oleic acid was supplied Adwic (Cairo, Egypt). Acetic acid and sodium hydroxide were laboratory grade chemicals. All the reagents used without further purification.

2.2. Methods

2.2.1. Synthesis of CS-ZnO composites

An exact amount of ZnO (0.25, 0.5, 0.75, or 1 g) was dissolved into 90 ml of acetic acid. 1 g of high molecular weight chitosan was then added the solution. 1% acetic acid was added to increase the volume to 100 ml. This viscous solution was then continuously stirred to fully dissolve the chitosan flakes, followed by sonication for 30 min. The pH of the solution was increased to 10 by the drop wise addition of 1 N NaOH. After heating in a water bath at 60 °C for about 3 h, and cooling to room temperature, the mixture was filtered and the obtained white precipitate was washed with distilled water several times. The resulting precipitate is dried at 60 °C for 1 h. Photoluminescence (PL) measurements determined the optimum weight of ZnO in this formulation to be 0.5 g.

2.2.2. Synthesis of CS-ZnO-oleic acid composites

0.5 g of ZnO was dissolved into 90 ml of acetic acid and then 1 g of high molecular weight chitosan was added to the solution. Oleic acid (0.5, 1, or 2 ml) was slowly added drop wise to the solution. 1% acetic acid was added to increase the volume to 100 ml. The rest of the synthetic procedure is identical to the synthesis of CS-ZnO. PL measurements determined the optimum volume of oleic acid in this formulation to be 1.0 ml.

2.2.3. Synthesis of the CS-ZnO-oleic:Eu^{3+} composite

0.5 g of ZnO and 0.05 g of Eu $(NO_3)_3$. $5H_2O$ were dissolved in 90 ml of 1% acetic acid. Then 1 g of chitosan was added and 0.5 ml of oleic acid slowly added drop wise to the solution. 1% acetic acid was added to increase the volume to 100 ml. The rest of the synthetic procedure is identical to the synthesis of CS-ZnO.

2.2.4. Printing paste preparation

The printing pastes were prepared with the following components:

Polyvinyl alcohol (PVA)	10 g
The luminescence material[a]	2 g
H_2O	88 g
	100 g

[a] The luminescent material was either pure ZnO, CS-ZnO NS, CS-ZnO-oleic QD or CS-ZnO:Eu^{3+} NR.

10 g of polyvinyl alcohol (PVA) was dissolved in 88 ml of hot water, and the solution then was stirred continuously to fully dissolve the PVA and give a clear viscous solution. 2 g of the luminescent material was then added and stirred until complete dissolution occurred.

2.3. Instrumentation

Identification of the crystal phases was conducted by X-ray diffraction analysis. The X-ray diffraction (XRD) patterns were obtained by using a Bruker-AXS D8 Advance, with Ni filtered Cu Kα radiation in the range of 2θ from 4 to 60. The reference data for the interpretation of the XRD patterns were obtained from the Joint Committee on Powder Diffraction Standards (JCPDS) files. Electron microscopy studies were undertaken using transmission electron microscopy (TEM) (JEOL JEM-1230, with an accelerating voltage of 40–120 kV) and scanning electron microscopy (SEM) (JEOL JXA-840A Electron Probe Microanalyzer, using an accelerating voltage of 30 kV) with an attached energy dispersive X-ray spectrometer (EDX). EDX measurements were acquired at a number of points in the samples. SEM samples were prepared on an appropriate disk and coated with gold to make the samples conductive to electrons.

Functional group determination was performed using infrared absorption spectra (IR) with a Nexus 670 FTIR spectrophotometer (Nicolet, Madison, WI, USA). The samples were mixed uniformly with potassium bromide in a 1:5 (sample:KBr) ratio. The KBr discs were prepared by compressing the mixed powders at a pressure of 5 tons for 5 min in a hydraulic press. The spectrum of the powder was recorded over a wave number range of 4000–400 cm^{-1}.

Luminescence spectra were measured in the range 254–800 nm using a Perkin Elmer LS 55. (PC) Spectrofluorophotometer with 3 nm excitation and emission slit width.

The colorimetric parameters of the printed cellulosic materials were determined on a reflectance spectrophotometer (UltraScan PRO D65, HunterLab, Virginia, USA).

3. Results and discussion

3.1. Structure

3.1.1. Fourier transform infrared spectroscopy

Fig. 1 shows the IR spectra of chitosan and the chitosan complexes. The characteristic peak at 3411 cm^{-1}, corresponding to the stretching vibration of —NH_2 and —OH of chitosan is shifted to higher frequencies (3419, 3455, and 3428 cm^{-1}) in the chitosan-ZnO, chitosan-ZnO-oleic and chitosan-ZnO-oleic:Eu^{3+} complexes. The peak at 1660 cm^{-1}, which is assigned to the bending vibration of the —NH_2 group present in chitosan was shifted to lower wavenumbers (1655, 1599 and 1595 cm^{-1}) in the chitosan-ZnO, chitosan-ZnO-oleic and chitosan-ZnO-oleic-Eu^{3+} complexes,

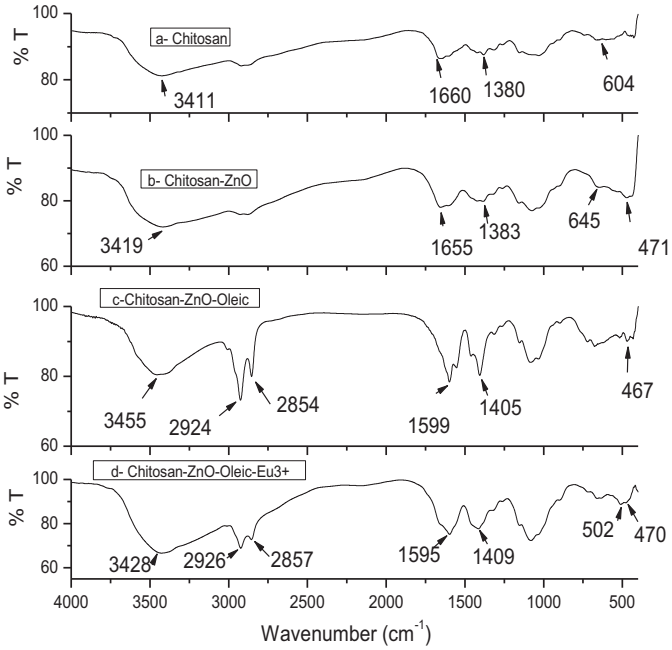

Fig. 1. FTIR spectra of (a) chitosan, (b) chitosan-Zn, (c) chitosan-ZnO-oleic and (d) chitosan-ZnO-oleic:Eu^{3+}.

respectively. This indicates that the —NH_2 and —OH groups of the chitosan are involved in complexation (Anadhavelu & Thambidurai, 2011).

The sharp absorption bands at 2854 and 2924 cm^{-1} (for chitosan-ZnO-oleic) are attributed to the C—H stretching vibration of the methylene chains ($(CH_2)_7$) and methyl (CH_3) groups of oleic acid (Li et al., 2010). These bands were shifted to 2857 and 2926 cm^{-1} (for chitosan-ZnO-oleic:Eu^{3+}). This indicates that the methylene chains and methyl groups of oleic acid are also involved in complexation.

The peaks between 670 and 1000 cm^{-1} can be assigned to the C—H bending vibration of the —HC═CH— moiety in oleic acid (Wen, Li, Liu, & Chen, 2011). The differences in some of these peaks indicate that a hydrogen bond can be formed between the —NH_2 and —OH of the chitosan groups and ZnO. The presence of new peaks at 471, 467 and 470 cm^{-1} in the chitosan-ZnO, chitosan-ZnO-oleic and chitosan-ZnO-oleic:Eu^{3+}, respectively, confirm chitosan-ZnO composite formation (Anadhavelu & Thambidurai, 2011).

3.1.2. X-ray diffraction spectrometry

Fig. 2 shows the XRD data of the chitosan and all composites synthesized from it. All of the XRD plots of the composites show peaks from the pure hexagonal structure of ZnO (JCPDS card No. 79-2205) (Chen & Gao, 2008; Xu & Du, 2003). Chitosan (Fig. 2a) exhibits two reflections that appear at $2\theta = 11^\circ$ and 20°, these two peaks correspond to the hydrated crystalline structure. These broad lines, especially for the higher diffraction angle ($2\theta \approx 20^\circ$), indicates that chitosan exhibits long-range chain order and that it is of high molecular weight (Srivastava, Tiwari, & Dutta, 2011). In the chitosan-ZnO, chitosan-ZnO-oleic and chitosan-ZnO-oleic:Eu^{3+} composites, the characteristic peak of chitosan at $2\theta = 11^\circ$ is weakened. This may be due to presence of ZnO particles which disturb (or impede) the order of polymer chain by interfering with the intermolecular hydrogen bonds and sterically (Anadhavelu & Thambidurai, 2011). This is especially pronounced if the chitosan used is of high molecular weight.

The peaks at $2\theta \approx 4.32^\circ$ and 6.5° in Fig. 2c and d are attributed to oleic acid (Smith & Heady, 1955). The XRD patterns of the chitosan-ZnO-oleic and chitosan-ZnO-oleic:Eu^{3+} exhibits greater peak broadening than the chitosan-ZnO, which is indicative of the ultra-small ZnO particle size in the composite.

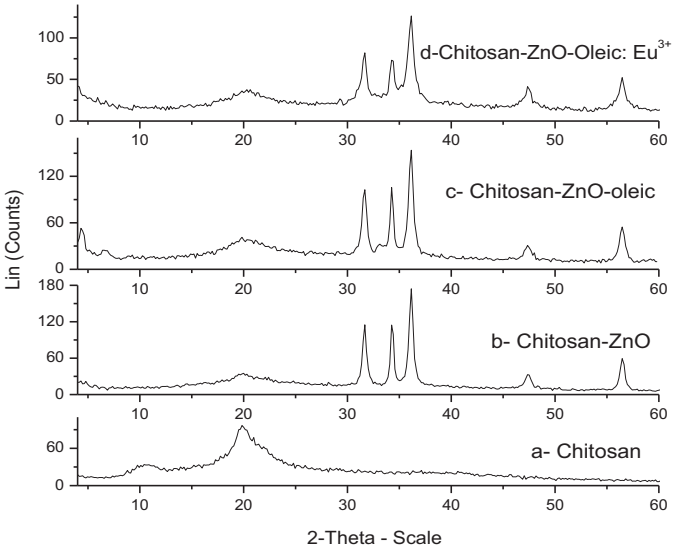

Fig. 2. XRD of (a) chitosan, (b) CS-ZnO, (c) CS-ZnO-oleic and (d) CS-ZnO-oleic:Eu^{3+}.

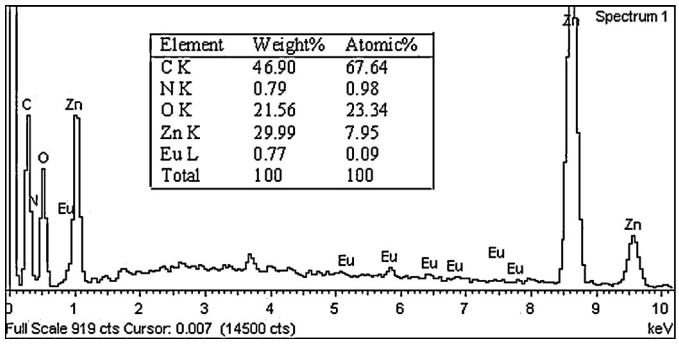

Fig. 3. EDX spectrum of the as synthesized CS-ZnO-oleic:Eu^{3+}.

The positions of the ZnO diffraction peaks hence the interplaner spacings (*d* values) are slightly shifted. This shift is attributed to the reaction of ZnO with the chitosan.

The XRD results therefore indicate the successful formation of ZnO nanocomposites.

3.1.3. Energy dispersed X-ray spectroscopy

The effective doping of Eu^{3+} ions into the prepared chitosan-ZnO-oleic:Eu^{3+} is confirmed by the EDX spectrum. As shown in Fig. 3, EDX spectra shows signals for oxygen, carbon, nitrogen, zinc, and europium. The elemental weight % of oxygen, carbon, nitrogen, zinc, and europium are 21.56, 46.9, 0.79, 29.99, and 0.77, respectively and are in good agreement with the expected theoretical weight %.

3.1.4. Transmission electron microscopy

Transmission electron microscopy investigations of the synthesized samples revealed differing morphologies (Fig. 4). The proposed growth mechanism of similar ZnO nanomaterials has been discussed in previous work by Li et al. (2012).

As can be seen in Fig. 4a, the CS-ZnO consists of heterogeneous nanospheres with average particle size of ~20 nm. Adding oleic acid during the CS-ZnO synthesis produces quantum dots (Fig. 4b) with an average particle size of 1–2 nm. Addition of the hydrophobic oleic acid prevents agglomeration and acts as appropriate hydrophilic coating around each of the particles to improve their suspension in the solvents and cause them to repel each other by columbic forces or steric hindrance. The high stability of quantum dots coated with oleic acid was attributed to the amorphous structure of the ligand layer. Similarly, branched ligands also deliver high chemical stability (Yan et al., 2011). Oleic acid protects the quantum dots, improving their suspension in water, stabilizing the reaction, and controlling growth (Sun, Lee, & Zhang, 2008).

Usually, pure ZnO grows preferentially along the [0 0 1] direction, under solvothermal conditions, because this facet has the lowest surface energy, because of this the rate of growth in the [0 1 0] direction is lower than that in the [0 0 1] direction (Hu, Li, Wong, Lee, & Lee, 2002; Xu & Sun, 2003). Using chitosan suppresses the growth along the c axis and nanospheres are formed. Incorporation of a Eu^{3+} dopant enhances the growth in the [0 0 1] direction forming nanorods (Fig. 4c).

3.2. Photoluminescence spectroscopy

Photoluminescence (PL) emissions of ZnO, CS-ZnO, CS-ZnO-oleic, and chitosan-ZnO-oleic:Eu^{3+} excited at 360 nm, are shown in Fig. 5. Pure ZnO exhibits emission bands at ~390, 420, 485, and 530 nm. The emission band around 390 nm results from a near-band-edge transition of the wide band gap of ZnO (Dutta, Ghosh, & Basak, 2009). Oxygen vacancies are essential defects in n-type ZnO and can capture electrons, thus forming ionized vacancies which

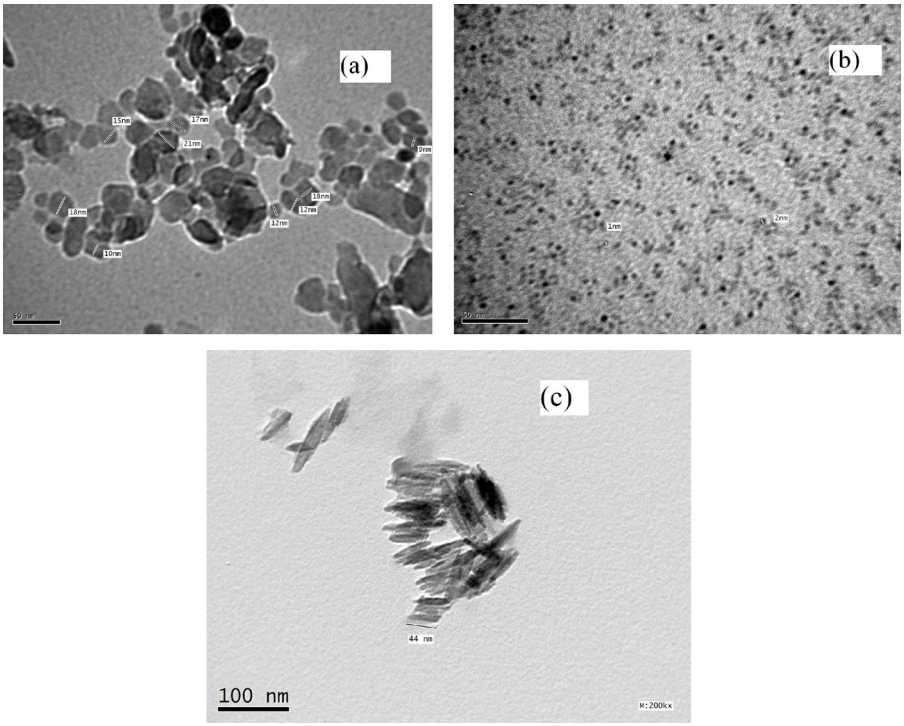

Fig. 4. TEM images of (a) CS-ZnO 300k×, (b) CS-ZnO-oleic 400k× and (c) CS-ZnO-oleic:Eu^{3+} 200k×.

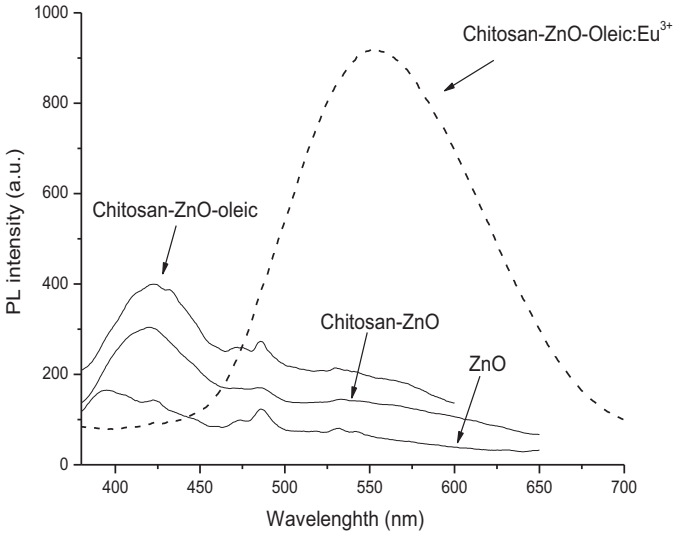

Fig. 5. Optimum photoluminescence emission spectra of ZnO, chitosan-ZnO, chitosan-ZnO-oleic, and chitosan-ZnO-oleic-Eu^{3+} excited at 360 nm.

act as deep defect donors and result in new energy levels, which further influences the optical properties of ZnO. The visible emission intensity at ~420 nm is attributed to the interstitial oxygen (induced recombination). The green emission at 485 nm may originate from the electron transition from the ionized oxygen vacancies level to the valence band (Gao, Li, & Yu, 2005). The emission at ~530 nm is most likely related to the deep-level (Baiqi et al., 2009).

It is obvious from Fig. 5 that Eu^{3+} doping of the chitosan-ZnO-oleic dramatically increases the luminescence intensity at 550 nm (with a red shift of 20 nm compared to the undoped samples). This is due to a change in energy band structure as a result of doping. Eu^{3+} doping is also known to improve surface states, and increase the number of defects and oxygen vacancies in ZnO (Trandafilović, Božanić, Dimitrijević-Branković, Luyt, & Djoković, 2012). Fig. 5 also shows that Eu^{3+} doping suppresses the other luminescence's of ZnO at ~390, 420 and 485 nm.

3.3. Color measurements

Various printing pastes containing the ZnO composites were prepared (as described in Section 2.2.4) and applied to cellulosic paper and cellulosic textile fabrics, using manual silk printing, in which uses a porous screen mounted onto wood frame. The basic principle of screen printing is that a stencil is applied to a mesh that is stretched over a rigid rectangular frame. The stencil inhibits ink from passing through all areas except where the stencil has been etched away. Printing paste is poured onto this mesh, and a squeegee forces the ink through the open areas in the stencil. The image is produced when the underside of the screen comes directly into contact with the material or substrate that is to be printed (paper or textile fabric). The used screen in this work is a design

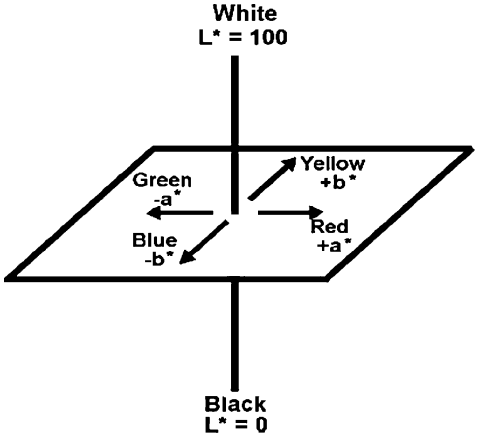

Scheme 1. CIE color space.

Table 1.1
Color values of unprinted, standard and printed Xerox paper.

	Xerox						
	K/S λ = 360	L^*	a^*	b^*	Whiteness index	Yellowness index	ΔE^*
Unprinted Xerox paper	0.94	90.38	1.96	−8.87	118.75	−17.21	–
Standard	1.06	90.16	2.01	−9.06	119.23	−17.62	–
ZnO printing	2.09	90.00	1.22	−6.57	107.32	−12.82	2.67
CS-ZnO-oleic printing	1.43	89.39	1.75	−7.75	111.77	−15.07	1.59
CS-ZnO-oleic:Eu^{3+} printing	1.07	89.50	1.87	−8.40	114.99	−16.39	0.99

containing stare image and the word “Nano”. The printed samples were dried at room temperature.

The standard is paper or fabric printed with PVA paste without any luminescent material.

The color of the printed cellulosic materials is expressed in terms of CIELAB values (Tables 1.1–1.5). All samples exhibited a λ_{max} = 360 nm.

Diffuse reflectance measurements were performed with an UltraScan PRO D65, HunterLab spectrophotometer, and the color values were calculated according to the Kubelka–Munk function (K/S) using the following equation (Battle, 1997):

$$\frac{K}{S} = \frac{(1-R)^2}{2R}$$

where K is the absorbance coefficient, S is the scattering coefficient and R is reflectance.

In the CIELAB system, the L^* value indicates the lightness of a color from 0 to 100. The chromatic axes, indicated by a^* and b^*, show the red-green and blue-yellow characteristics of color (Scheme 1) (Ohno, 2000). The maximum value of L^* is 100, which represents a prefect reflecting diffuser. The minimum L^* is zero and signifies black. The other (horizontal) axes are represented by a^* and b^*. These are at right angles to each other and cross in the center. It is based on the principle that a color cannot be both red and green, or blue and yellow. The a^* and b^* have no specific numerical limits. A positive of a^* is red, a negative value of a^* is green, a positive value of b^* is yellow and a negative of b^* is blue (CIE, 2004; Ohno, 2000). All of this is summarized in Scheme 1.

The color difference (ΔE^*) in the CIELAB space is calculated as the Euclidean distance between the points in this three-dimensional space, and is given by the following equation (Robertson, 1977):

$$\Delta E* = (\Delta L*^2 + \Delta a*^2 + \Delta b*^2)^{0.5}$$

where $\Delta L^* = L^*_{SMP} - L^*_{STD}$, $\Delta a^* = a^*_{SMP} - a^*_{STD}$ and $\Delta b^* = b^*_{SMP} - b^*_{STD}$.

Whiteness is defined as being an attribute of visual sensation of those colors, perceived by the human eyes as being white, that appear to be void of any hue and grayness. Whiteness index (WI) and yellowness index (YI) were determined according the American Society for Testing and Materials (E313 method). The calculated data is based on D65 illumination and 10-degree observation (ASTM. E313, 2005).

Tables 1.1–1.3 show the color values of Xerox, Rakta and Quena, respectively. The color values of cotton and linen textile fabrics are shown in Tables 1.4 and 1.5, respectively.

The color of the printed cellulosic materials values (Tables 1.1–1.5) show that printing causes a slight decrease in lightness (L^*) and because of this whiteness is also decreased.

Table 1.2
Color value of unprinted, standard and printed Rakta paper.

	Rakta						
	K/S λ = 360	L^*	a^*	b^*	Whiteness index	Yellowness index	ΔE^*
Unprinted Rakta paper	3.96	84.89	−1.26	9.39	18.77	17.82	–
Standard	5.62	80.72	−1.22	10.62	2.48	21.0	–
ZnO printing	6.02	82.75	−1.41	12.16	−0.57	23.36	2.34
CS-ZnO-oleic printing	5.83	81.66	−1.21	11.71	−0.92	22.92	1.52
CS-ZnO-oleic:Eu^{3+} printing	5.51	82.67	−1.33	11.36	3.35	21.93	1.66

Table 1.3
Color value of unprinted, standard and printed Quena paper.

	Quena						
	K/S λ = 360	L^*	a^*	b^*	Whiteness index	Yellowness index	ΔE^*
Unprinted Quena paper	1.48	92.05	1.64	−8.67	120.90	−16.75	–
Standard	1.79	90.52	1.94	−8.97	119.47	−17.42	–
ZnO printing	3.15	91.13	1.09	−6.53	109.3	−12.7	2.56
CS-ZnO-oleic printing	1.53	91.52	1.45	−7.68	115.38	−14.85	1.68
CS-ZnO-oleic:Eu^{3+} printing	1.82	91.31	1.79	−8.75	119.87	−16.92	0.92

Table 1.4
Color value of unprinted, standard and printed Cotton fabric.

	Cotton						
	K/S λ = 360	L^*	a^*	b^*	Whiteness index	Yellowness index	ΔE^*
Unprinted cotton fabric	0.16	84.16	−0.29	0.98	60.33	1.82	–
Standard	0.18	84.11	−0.29	1.05	59.00	1.96	–
ZnO printing	1.22	80.97	−0.17	0.96	53.44	1.94	3.26
CS-ZnO-oleic printing	0.43	83.52	−0.22	1.66	54.73	3.34	0.88
CS-ZnO-oleic:Eu^{3+} printing	0.34	83.64	−0.35	1.65	55.01	3.21	0.77

Table 1.5
Color value of unprinted, standard and printed Linen fabric.

	Linen						
	K/S λ = 360	L^*	a^*	b^*	Whiteness index	Yellowness index	ΔE^*
Unprinted linen fabric	0.46	83.39	−0.6	5.9	27.85	13.79	–
Standard	0.61	81.81	−0.56	7.73	20.08	15.68	–
ZnO printing	1.72	82.09	−0.55	6.66	26.22	13.50	1.09
CS-ZnO-oleic printing	0.65	82.42	−0.52	6.72	26.60	13.62	1.16
CS-ZnO-oleic:Eu^{3+} printing	0.55	82.81	−0.56	6.34	29.41	12.77	1.69

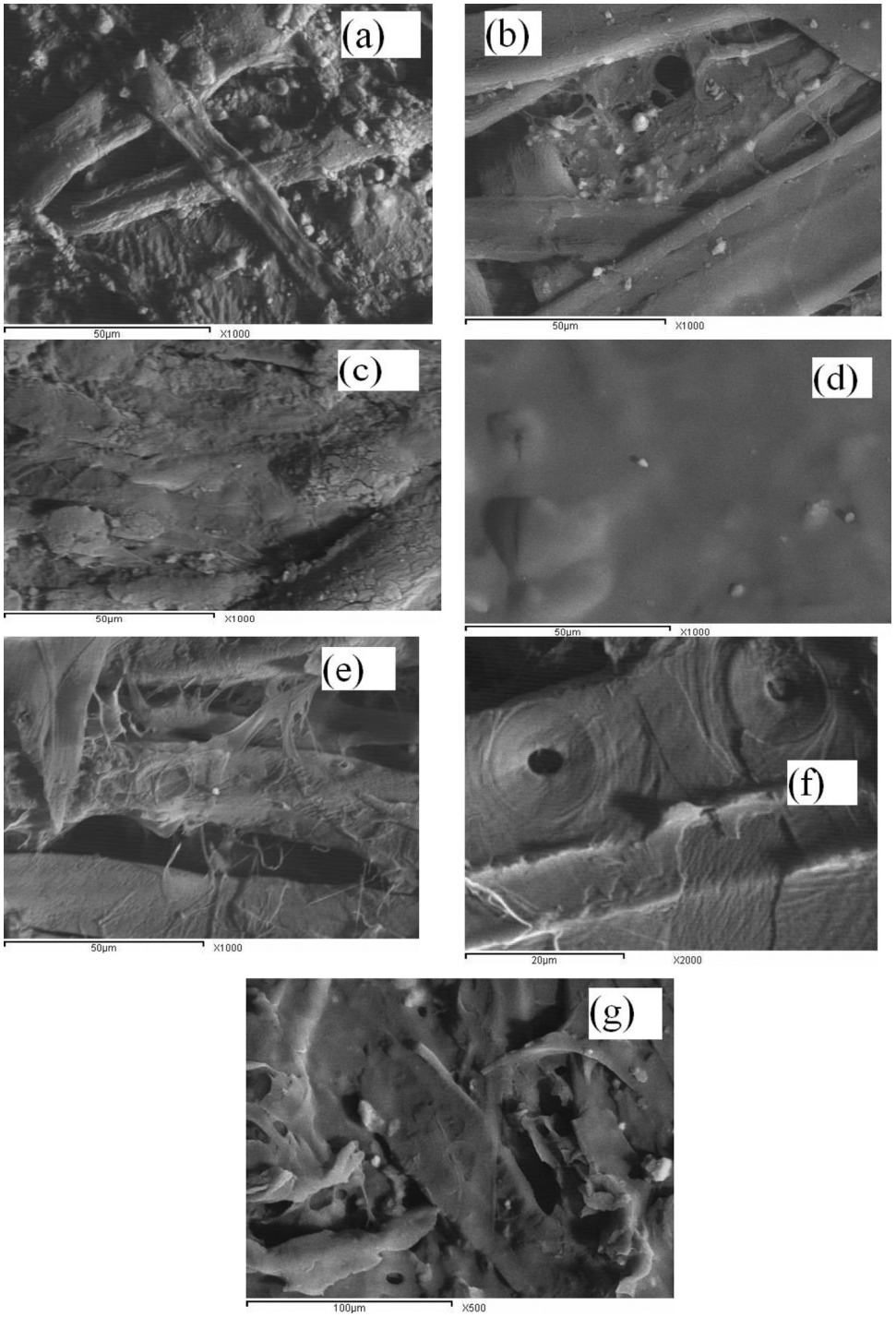

Fig. 6. SEM images of (a) unprinted Xerox paper 1000×, (b) printed Xerox paper 1000×, (c) unprinted Quena paper1000×, (d) printed Quena paper 1000×, (e) unprinted Rakta paper 500×, (f) unprinted Rakta paper 2000× and (g) printed Rakta paper 1000×.

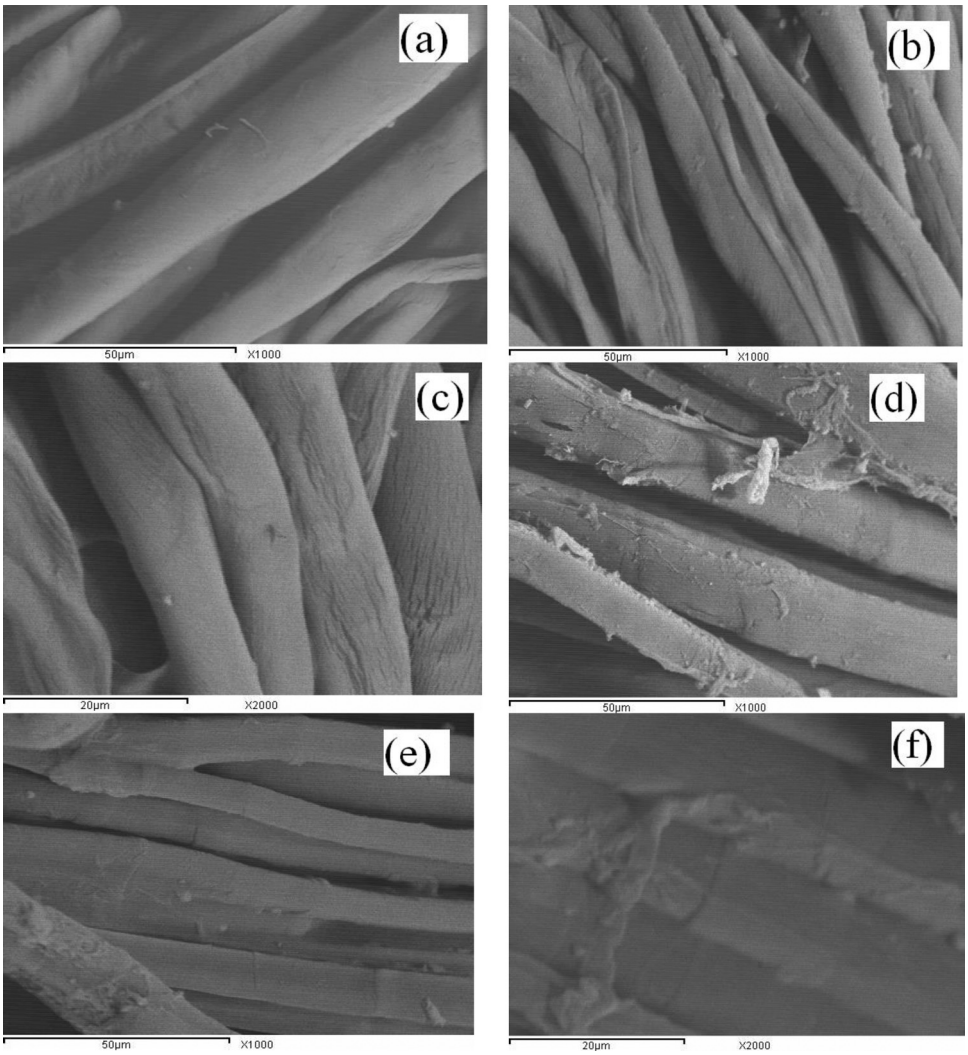

Fig. 7. SEM images of (a) unprinted cotton fabric 1000×, (b) printed cotton fabric 1000×, (c) printed cotton fabric 2000×, (d) unprinted linen fabric 1000×, (e) and printed linen fabric 1000× and (f) printed linen fabric 2000×.

This slight decrease indicates that the printed layer is transparent and thin. The scanning electron microscopy (SEM) images (Figs. 6 and 7) of all the printed surfaces also confirm that this layer is thin. The fluorescence emission of the nanocomposites increases the perception of whiteness and brightness.

The color difference (ΔE^*) in all printed samples is less than 4 and so this printing layer is considered invisible to the untrained eye (the majority of people) (Bala & Klassen, 2003; Zielnik, 2006). In case the of the CS-ZnO-oleic and CS-ZnO-oleic:Eu^{3+} printed samples, ΔE^* is less than 2, this indicates that the printed layer would be invisible even to a trained eye (experienced observer). Therefore printing with CS-ZnO-oleic and CS-ZnO-oleic:Eu^{3+} ink may be suitable as security features in paper and textile tagging.

If we are going to use labeled ink in high-quality products like banknotes, printing quality needs to be of the highest standard. Because of this SEM studies were carried out on various paper and textile surfaces, using CS-ZnO-oleic:Eu^{3+} as ink. Both the printed and unprinted surfaces were imaged.

3.4. Scanning electron microscopy

The SEM image of unprinted Xerox paper is shown in Fig. 6a, the surface of the fibers is coated with aggregates of the filler agent. Upon printing with ink (Fig. 6b), this filler agent is then obviously coated with the printed layer.

Fig. 6c shows the fibers of the bagasse pulp in Quena paper. The fibers are coated with filler and sizing agent aggregates, this paper sheet is denser, with many fibers per unit area, and only a few voids exist between the fibers. This coating reduces printing paste absorption, and so the printed surface layer (Fig. 6d) is the thickest compared to the other printed papers.

Fig. 6e and f shows the SEM image of unprinted Rakta absorbing paper, which is made from rice straw pulp. The fibers are less densely packed, and there are a many voids on the surfaces, and obvious pitting, which leads to higher absorption of printing paste (El-Molla, Shama, & Saeed, 2013). The printed surface layer of this paper (Fig. 6g) has a thinner layer than either Xerox or Quena paper.

The SEM image of unprinted (the original) cotton fiber (Fig. 7a) shows convolution of the cotton fiber. The fiber surface is smooth with voids between the fibers. The surface of the printed cotton textile fabric (Fig. 7b) appears quite smooth at low magnifications (1000×). This may be due to the highly absorbent nature of cotton textile fabrics, meaning that the printed layer penetrates to the depth of the fiber. This is confirmed by looking at the printed surface at high magnifications (Fig. 7c); a thin printed layer is observed.

From the SEM image of the unprinted linen fiber (Fig. 7d), many rough, small fibers, that protrude from the woven threads,

and become intertwined with other fibrils from other threads, are observed. When comparing this with the SEM image of the unprinted cotton fiber, the linen fabric surface looks denser, with more fibers per unit area, and fewer voids between the fibers. All of the SEM images of these printed surfaces show that the printed layer is thin and therefore suitable for use as a luminescent security feature.

4. Conclusion

This work reports on a facile and novel method for the preparation of different CS-ZnO nanocomposites. Eu^{3+} doping of CS-ZnO-oleic leads to a remarkable increase in the visible photoluminescence intensity at 550 nm.

The TEM studies of the synthesized samples showed formation of different nanoshapes. CS-ZnO exists as heterogeneous nanospheres, CS-ZnO-oleic as quantum dots and CS-ZnO:Eu^{3+} as nanorods.

The prepared luminescent CS-ZnO nanomaterials were formulated in a printing paste and applied to different types of papers and textiles using a screen-printing technique. The colorimetric values of the printed CS-ZnO-oleic acid and CS-ZnO-oleic:Eu^{3+} papers showed only a slight change in color difference (ΔE^*) and also in the color parameters: L^*, a^* and b^*. SEM studies of the printed surface showed that the printed layer is thin. These data indicate that highly luminescent CS-ZnO-oleic and highly luminescence CS-ZnO-oleic:Eu^{3+} nanocomposites are suitable for use as a printed security feature.

References

Anadhavelu, S., & Thambidurai, S. (2011). Preparation of chitosan-zinc oxide complex during chitin deacetylation. *Carbohydrate Polymers*, *83*, 1565–1569.

ASTM. E313. (2005). *Standard practice for calculating yellowness and whiteness indices from instrumentally measured color coordinates*. http://dx.doi.org/10.1520/E0313-05

Baiqi, W., Xudong, S., Qiang, F., Iqbal, J., Yan, L., Honggang, F., et al. (2009). Photoluminescence properties of Co-doped ZnO nanorods array fabricated by the solution method. *Physica E*, *41*(3), 413–417.

Bala, R., & Klassen, R. V. (2003). *Digital color imaging: Handbook*. Boca Raton, FL, USA: CRC Press, Inc.

Battle, D. R. (1997). In R McDonald (Ed.), *Colour physics for industry* (pp. 1–56). Bradford, England: Society of Dyers and Colourists.

Chan, W. C. W., Maxwell, D. J., Gao, X., Bailey, R. E., Han, M., & Nie, S. (2002). Luminescent quantum dots for multiplexed biological detection and imaging. *Current Opinion in Biotechnology*, *13*(1), 40–46.

Chen, Z., & Gao, L. (2008). A new route toward ZnO hollow spheres by a base-erosion mechanism. *Crystal Growth and Design*, *8*(2), 460–464.

CIE. (2004). *Technical report, colorimetry* (3rd ed., pp. 6–20). Vienna, Austria: Bureau Central de la CIE [CIE Pub. No. 15.3].

Dutta, M., Ghosh, T., & Basak, D. (2009). N doping and Al-N co-doping in sol–gel ZnO films: Studies of their structural, electrical, optical, and photoconductive properties. *Journal of Electronic Materials*, *38*(11), 2335–2342.

El-Molla, M. M., Shama, S. A., & Saeed, E-S. S. (2013). Preparation of disappearing inks and studying the fading time on different paper surfaces. *Journal of Forensic Sciences*, *58*(1), 188–194.

Gao, M. D., Li, M. M., & Yu, W. D. (2005). Flowerlike ZnO nanostructures via hexamethylenetetramine-assisted thermolysis of zinc-ethylenediamine complex. *Journal of Physical Chemistry B*, *109*(3), 1155–1161.

Hall-Goulle, V. (2006). *Ink compositions containing lanthanide complexes*. United States Patent, USP 7,108,742.

Hardwick, B., Jackson, W., Wilson, G., & Mau, A. W. H. (2001). Advanced materials for banknote applications. *Advanced Materials*, *13*(12), 980–984.

Hu, J. Q., Li, Q., Wong, B., Lee, C. S., & Lee, S. T. (2002). Synthesis of uniform hexagonal prismatic ZnO whiskers. *Chemistry of Materials*, *14*(3), 1216–1219.

Ikeda, M., Kitayama, Y., Kiyoyanagi, N., & Shirasaki, Y. (2006). *Europium compounds and ink compositions containing the same*. United States Patent, USP 145122.

Imanishi, K., & Yamasaki, Y. (2003). *Red luminous ink composition*. European Patent, EP 1277811.

Li, C., Du, X., Lu, W., Liu, K., Chang, J., Chen, S., et al. (2012). Luminescent single-crystal ZnO nanorods: Controlled synthesis through altering the solvents composition. *Materials Letters*, *81*(15), 229–231.

Li, D., Jiang, D., Chen, M., Xie, J., Wu, Y., Dang, S., et al. (2010). An easy fabrication of monodisperse oleic acid-coated Fe_3O_4 nanoparticles. *Materials Letters*, *64*(22), 2462–2464.

Morrison, S. (2009). *Standard catalog of world paper money* (15th ed.). Wisconsin: Krause Publications, Inc.

Mosquera, A. A., Horwat, D., Rashkovskiy, A., Kovalev, A., Miska, P., Wainstein, D., et al. (2013). Exciton and core-level electron confinement effects in transparent ZnO thin films. *Scientific Reports*, *3* http://dx.doi.org/10.1038/srep01714 (Article number: 1714)

Muzzarelli, R. A. A. (2011). Potential of chitin/chitosan-bearing materials for uranium recovery: An interdisciplinary review. *Carbohydrate Polymers*, *84*, 54–63.

Ohno, Y. (2000). *CIE Fundamentals for Color Measurements, Paper for IS&T NIP16: International Conference on Digital Printing Technologies Conference* Vancouver, Canada, (pp. 540–545).

Prime, E. L., & Solomon, D. H. (2010). Australia's plastic banknotes: Fighting counterfeit currency. *Angewandte Chemie International Edition*, *49*, 3726–3736.

Riva, R., Ragelle, H., des Rieux, A., Duhem, N., Jerome, C., & Preat, V. (2011). Chitosan and chitosan derivatives in drug delivery and tissue engineering. *Advance in Polymer Science*, *244*, 19–44.

Robertson, A. R. (1977). The CIE 1976 colour difference formula. *Color Research and Application*, *2*, 7–11.

Smith, H. N., & Heady, H. H. (1955). Identification of frozen liquid samples with the X-ray diffractometer. *Analytical Chemistry*, *27*(6), 883–888.

Smith, A. M., & Nie, S. (2010). Semiconductor nanocrystals: Structure, properties, and band gap engineering. *Accounts of Chemical Research*, *43*(2), 190–200.

Srivastava, R., Tiwari, D. K., & Dutta, P. K. (2011). 4-(Ethoxycarbonyl) phenyl-1-amino-oxobutanoic acid-chitosan complex as a new matrix for silver nanocomposite film: Preparation, characterization and antibacterial activity. *International Journal of Biological Macromolecules*, *49*(5), 863–870.

Sun, C., Lee, J. S., & Zhang, M. (2008). Magnetic nanoparticles in MR imaging and drug delivery. *Advanced Drug Delivery Reviews*, *60*, 1252–1265.

Trandafilović, L. V., Božanić, D. K., Dimitrijević-Branković, S., Luyt, A. S., & Djoković, V. (2012). Fabrication and antibacterial properties of ZnO–alginate nanocomposites. *Carbohydrate Polymers*, *88*, 263–269.

Wang, X., Xu, S., & Xu, W. (2011). Luminescent properties of dye–PMMA composite nanospheres. *Physical Chemistry Chemical Physics*, *13*, 1560–1567.

Wang, N., Yang, Y., & Yang, G. (2011). Great blue-shift of luminescence of ZnO nanoparticle array constructed from ZnO quantum dots. *Nanoscale Research Letters*, http://dx.doi.org/10.1186/1556-276X-6-338

Wen, J., Li, J., Liu, S., & Chen, Q. Y. (2011). Preparation of copper nanoparticles in a water/oleic acid mixed solvent via two-step reduction method. *Colloids and Surfaces A: Physicochemical and Engineering Aspects*, *373*(1), 29–35.

Xu, Y., & Du, Y. (2003). Effect of molecular structure of chitosan on protein delivery properties of chitosan nanoparticles. *International Journal of Pharmaceutics*, *250*(1), 215–226.

Xu, C. X., & Sun, X. W. (2003). Characteristics and growth mechanism of ZnO whiskers fabricated by vapor phase transport. *Japanese Journal of Applied Physics*, *42*, 4949–4952.

Yan, E., Wang, C., Wang, S., Sun, L., Wang, Y., Fan, L., et al. (2011). Materials synthesis and characterization of fluorescent chitosan-ZnO hybrid nanospheres. *Materials Science and Engineering B*, *176*, 458–461.

Zielnik, A. (2006). Durability: Keeping up appearances. *Journal of Architectural Coatings*, (February/March), 62–67.